FIB lift-out of conducting ferroelectric domain walls in hexagonal manganites

Aleksander B. Mosberg (iD), Erik D. Roede (iD), Donald M. Evans (iD), Theodor S. Holstad (iD), Edith Bourret (iD), Zewu Yan (iD), Antonius T. J. van Helvoort (iD), and Dennis Meier (iD)

View Online   Export Citation   CrossMark

ARTICLES YOU MAY BE INTERESTED IN

FIB lift-out of conducting ferroelectric domain walls in hexagonal manganites

Aleksander B. Mosberg,[1,a)] (iD) Erik D. Roede,[2] (iD) Donald M. Evans,[2,b)] (iD) Theodor S. Holstad,[2] (iD) Edith Bourret,[3] (iD)
Zewu Yan,[4] (iD) Antonius T. J. van Helvoort,[1] (iD) and Dennis Meier[2] (iD)

AFFILIATIONS

[1]Department of Physics, Norwegian University of Science and Technology (NTNU), 7491 Trondheim, Norway
[2]Department of Materials Science and Engineering, Norwegian University of Science and Technology (NTNU), 7491 Trondheim, Norway
[3]Materials Sciences Division, Lawrence Berkeley National Laboratory, Berkeley, California 94720, USA
[4]Department of Physics, ETH Zurich, Otto-Stern-Weg 1, 8093 Zurich, Switzerland

a)aleksander.b.mosberg@ntnu.no
b)donald.evans@ntnu.no

ABSTRACT

A focused ion beam (FIB) methodology is developed to lift out suitable specimens containing charged domain walls in improper ferroelectric $ErMnO_3$. The FIB procedure allows for extracting domain wall sections with well-defined charge states, enabling accurate studies of their intrinsic physical properties. Conductive atomic force microscopy (cAFM) measurements on a 700 nm thick lamella demonstrate enhanced electronic transport at charged domain walls consistent with previous bulk measurements. A correlation is shown between domain wall currents in cAFM and applied ion beam polishing parameters, providing a guideline for further optimization. These results open the door for the study and functionalization of individual domain walls in hexagonal manganites, an important step toward the development of atomic scale domain-wall devices that can operate at low energy.

Published under license by AIP Publishing. https://doi.org/10.1063/1.5115465

Ferroelectric domain walls hold great potential as ultrasmall functional elements for future nanotechnology.[1–4] The functionality of the domain walls originates from their distinct symmetry combined with their sensitivity to electrostatics and strain, leading to unusual physical properties beyond bulk properties. For example, electrically conducting domain walls arise in a wide variety of otherwise insulating ferroelectrics, including proper and improper ferroelectrics [proper: $BiFeO_3$,[5] $PbZr_{0.2}Ti_{0.8}O_3$,[6] $LiNbO_3$,[7] and $BaTiO_3$;[8] improper: $RMnO_3$ (R = Sc, Y, Dy-Lu),[9,10] $Cu_3B_7O_{13}Cl$,[11] and $(Ca,Sr)_3Ti_2O_7$[12]].

Hexagonal manganites are particularly intriguing as they naturally develop all orientations of ferroelectric 180° domain walls, namely, neutral, positively charged (head-to-head), and negatively charged (tail-to-tail) walls.[9] This coexistence allows for systematic studies of the unusual and complex nanoscale physics at charged domain walls.[4,9,10,13,14] Additionally, the different domain walls can give rise to functionalities beyond just conductance, acting, e.g., as atomic-scale capacitors,[15,16] digital switches,[17] and diodes.[18]

However, the scientific and technological merit of the domain walls in hexagonal manganites is strongly limited by the difficulty of adequately accessing and measuring individual domain walls with a well-defined charge state. Until now, all domain-wall related transport studies have been performed at the surface of single crystal bulk samples, mapping relative differences in conductance. As the walls strongly meander within the bulk and, hence, continuously vary their charge state, such measurements include a largely unknown electronic background from subsurface domains and domain walls.[19] A standard procedure to mitigate this problem is to resort to thin films, where it is more likely that walls connect from top to bottom without changing orientation. In hexagonal manganite thin films, however, the typical domain size is on the order of ~20 nm,[20] i.e., below the resolution limit of the scanning probe microscopy (SPM) methods commonly used to study them, thus prohibiting the characterization of electronic properties at individual domain walls.

An alternative approach to achieve thin enough specimens is to use a focused ion beam (FIB), milling and lifting out thin lamella specimens.[21] FIB has been used with great success for nanopatterning and domain engineering in a variety of proper ferroelectrics.[22–27] The approach has never been used, however, to extract individual domain

walls from improper ferroelectric bulk samples under the explicit condition of keeping their original electronic properties and functionality. Furthermore, when working with hexagonal manganites, otherwise standard postprocessing procedures, such as annealing to remove the FIB-induced damage layer from the lamella, become critical:[28] in RMnO$_3$, annealing is known to reconfigure the electronic bulk properties,[29] making it difficult to ensure that domain wall structures in the lamella correspond to their original bulk counterparts.

In this work, an *in situ* lift-out methodology is presented that allows for FIB preparation of hexagonal manganite (ErMnO$_3$) lamellas without the need for postprocessing (e.g., annealing). Scanning electron microscopy (SEM) and SPM imaging demonstrate that the characteristic domains and domain wall properties of bulk ErMnO$_3$ are preserved in the FIB-milled lamella, revealing charged domain walls with enhanced electronic conductance. Additionally, the optimization potential in FIB polishing is explored by examining how different FIB polishing conditions correlate with conductance contrast at the domain walls. It is shown that a 5 kV polishing step greatly and reversibly enhances conductance contrast at domain walls in a 700 nm thick lamella.

A lamella is prepared from a hexagonal ErMnO$_3$ single crystal grown using the pressurized floating zone method[30] and cut to achieve a sample surface with out-of-plane polarization ($P||[001]$). The crystal is chemomechanically polished to give a root mean square roughness of ≤ 10 nm and coated with a thin (20 nm) layer of platinum to prevent excessive charging and drift at higher beam currents for both the electron and ion beams. The sample is loaded in a Thermo Fisher Scientific Helios Nanolab G4 DualBeam FIB system, where SEM inspection of the sample surface [as shown for a representative uncoated sample in Fig. 1(a)] confirms the presence of domain contrast[31–34] matching the characteristic domain structure of hexagonal manganites, imaged by piezoresponse force microscopy (PFM) in Fig. 1(b). Following conventional *in situ* lift-out lamella preparation methods for transmission electron microscopy,[35] an $\sim$1 μm thick lamella is milled out and polished with a 30 kV 90 pA ion beam. At this point, the domain structure of both lamella faces [Fig. 1(c)] can be observed, and by comparing the domain structures of both sides as highlighted with a manually traced overlay in Fig. 1(d), it is possible to identify which domain walls have a high probability of penetrating the lamella without significant changes in orientation (and related charge states).[9] The approach for estimating the domain wall orientation is presented in supplementary material Note 1.

For SPM characterization, the lamella is then lifted out using an EasyLift EX lift-out needle. Using a combination of motorized needle rotation and a pretilt stub, it is possible to put down the lamella in a single step, i.e., without any transfer steps as commonly used in plan-view lamella preparation (which requires a similar 90° rotation between the plan-view and cross-sectional geometry[36]). This process is illustrated in Fig. 2: the needle is attached [Fig. 2(a)] so that when rotated 180° around the needle axis, the lamella can be placed flat and fastened with deposited C strips on a substrate suitable for SPM. For this work, a MgO substrate is used, covered with 300 nm Pt [Fig. 2(b)] to serve as the back electrode. By mounting the substrate on a pretilted stub at a 45° stage tilt [Fig. 2(c)], the glancing incident angles desired for optimal ion beam polishing can be achieved by simply tilting the stage down to $10° - 12°$ [Fig. 2(d)].

At this point, the lamella is thinned to approximately 700 nm and polished with the 30 kV beam at a glancing angle of 3°–5°.
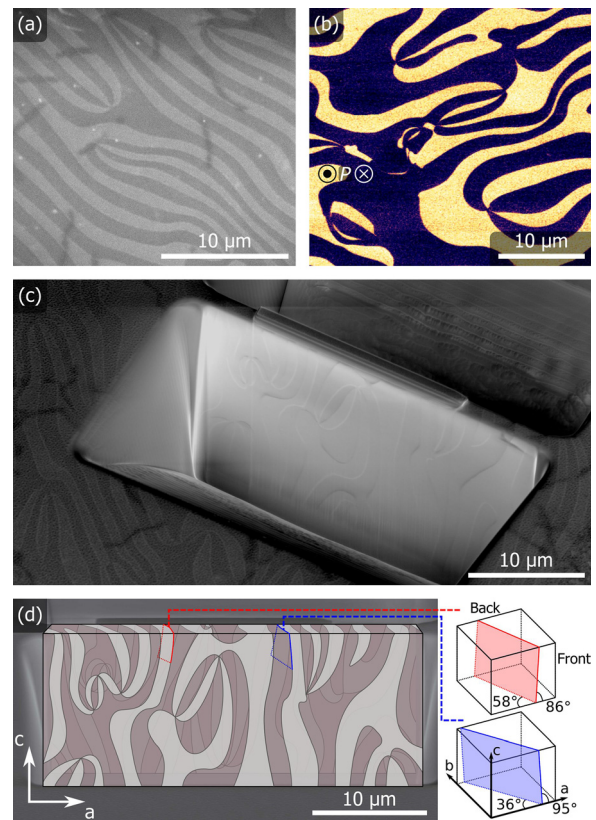
FIG. 1. Domain structure in hexagonal manganites. (a) 3 kV SEM secondary electron image of ferroelectric domains in ErMnO$_3$ (out-of-plane polarization). (b) Reference PFM image (71 kHz; 20 V peak-to-peak) of the domain structure, recorded on a ErMnO$_3$ crystal from the same growth batch. (c) SEM of the lamella in trench with an observable domain structure. (d) SEM image of the lamella cross section with the overlay depicting the observed domain structure from both sides and top of the lamella. Two domain wall segments are highlighted with approximate geometry through the lamella using a lamella coordinate system abc, with c || P.

Note that the bottom contact of the lamella must be milled flat and polished before lift-out.

The lamella, as shown topographically by SEM backscatter contrast in Fig. 3(a) and with secondary electron domain wall contrast in Fig. 3(b), is then loaded in a NT-MDT Ntegra Prima SPM and examined using PFM and conductive atomic force microscopy (cAFM). PFM is acquired using a MikroMasch NSC35/Pt probe with a peak-to-peak AC voltage of 20 V and a frequency of 32.1 kHz [Fig. 3(c)]. Dark and bright areas correspond to domains that on the lifted-out lamella have in-plane ferroelectric polarization pointing up and down, respectively. cAFM scans are recorded from the same area as the SEM and PFM data in Figs. 3(b) and 3(c), with a voltage of 15 V [Fig. 3(d)] applied to the back electrode (probe tip: TipsNano DCP20). All three imaging techniques cross-correlate well with each other and reveal that the lamella retains the same domain pattern as the ErMnO$_3$ single crystal from which it has been lifted out. Most importantly for the scope of this work, the cAFM image demonstrates enhanced conductance at both tail-to-tail and head-to-head domain walls. The latter is in agreement with cAFM measurements on ErMnO$_3$ bulk samples,[17]
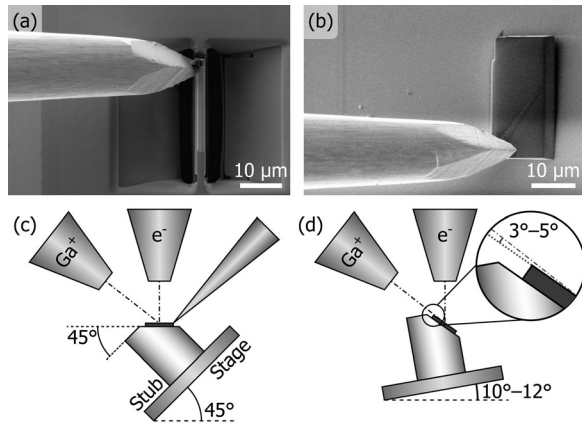
FIG. 2. Lift-out methodology. (a) SEM image of the lift-out needle position before rotation. (b) Specimen lifted out, rotated 180° around the needle axis, and placed on the substrate. (c) and (d) Schematic of the lift-out setup with pretilted stub and stage tilt when putting down the lamella (c), allowing for milling at glancing angles in (d).

indicating a minimally invasive specimen preparation. More details on domain wall currents can be found in supplementary material Note 2.

However, the voltage required to record conductance maps, such as in Fig. 3(d) (15 V), is higher than the few millivolts expected assuming that field strength scales linearly with the thickness.[17] This difference is likely due to surface damage layers from FIB-milling as illustrated in Fig. 4(a). Such FIB-induced damage is largely dominated by Ga implantation and amorphization, and multiple strategies exist to limit its impact.[37] Notably, reducing ion beam energy is known to reduce the damage layer thickness[37,38] at the cost of milling yield.
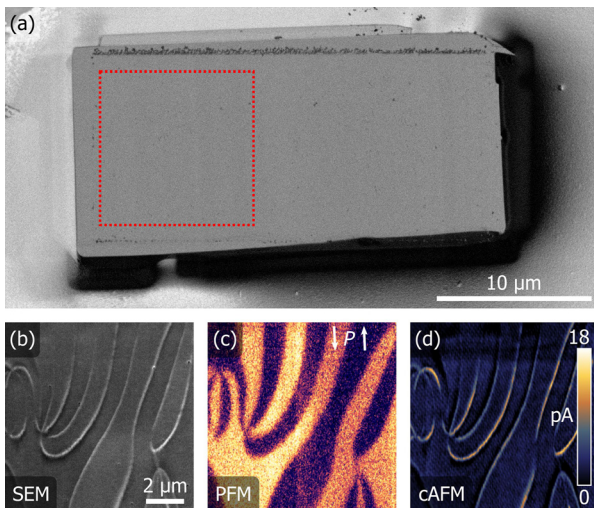
FIG. 3. SEM, PFM, and cAFM contrast on the lamella. (a) 2 kV SEM backscatter image of lamella topography. (b) Corresponding secondary electron image, from the region marked in (a), with domain wall contrast. (c) PFM (20 V peak-to-peak, 32.1 kHz) of the same region with the domain structure and the polarization direction marked by arrows. (d) Corresponding cAFM scan (15 V) with domain wall contrast matching (b).
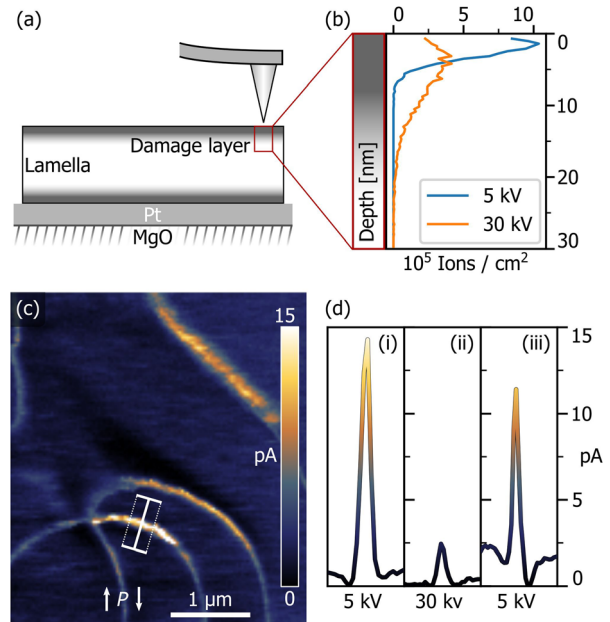
FIG. 4. Effect of the damage layer thickness on cAFM. (a) Schematic cross section of the lamella with FIB damage layers. (b) Ga implantation profiles from FIB polishing at 5 and 30 kV as simulated in TRIM (15 000 ions, 3° incident angle). (c) cAFM scan (10 V) of a conducting tail-to-tail domain wall on the lamella, 5 kV polished. (d) Conductance profiles over the 10 pixel wide domain wall section highlighted in (c). Profiles shown for 5 kV polished (i), 30 kV milled (ii), and 5 kV repolished (iii) lamellas, extracted from similar cAFM scans at 10 V (individual scans are shown in supplementary material Fig. S3).

Reduction in the damage layer thickness is expected to greatly improve imaging conditions for SPM techniques such as cAFM which are highly surface sensitive. A first approximation[39] for this change in the damage layer thickness can be shown by comparing Ga implantation profiles for different incident beam energies [Fig. 4(b)]. Profiles are simulated in TRIM[40] for stoichiometric $ErMnO_3$ with a density of $7.29\,g\,cm^{-3}$, for 5 kV and 30 kV Ga beams at an incident angle of 3°.

To further understand the impact of the damage layer on detected domain wall currents and establish guidelines toward optimized FIB polishing conditions, the lamella is polished multiple times using two different ion beam energies. Between each polishing step, a cAFM scan is performed to provide a comparison. Lamella height profiles (measured relative to the substrate) are also recorded to measure how much material each polishing step has milled. It is verified that this milling depth is larger than the implantation profiles in Fig. 4(b) to ensure that the previous damage layer has been completely removed. A cAFM scan taken after polishing with a 5 kV beam is shown in Fig. 4(c). Panel (i) of Fig. 4(d) presents the corresponding current profile measured across the single tail-to-tail domain wall marked in Fig. 4(c). After mapping the domain wall conductance, the lamella is milled with 30 kV (removing approximately 60 nm) and the cAFM measurement is repeated [Fig. 4(d) (ii)]. Finally, the lamella is repolished with 5 kV (removing approximately 35 nm) and the profile shown in Fig. 4(d) (iii) is taken.

Because each polishing step necessarily includes milling away of enough material to remove the previous damage layer, the domain

wall position can vary slightly between the cAFM scans. As a consequence, contributions due to variations in the domain wall charge state can differ in Fig. 4(d). Nevertheless, the comparison of the current profiles clearly reveals a correlation between polishing voltage and the effective conductance measured at the tail-to-tail walls. Notably, the conductance contrast at tail-to-tail walls is reduced approximately by a factor of 5 when measured through the thicker damage layer from being milled with 30 kV (ii) compared to milling at 5 kV (i). After repolishing with 5 kV, a contrast level comparable to the initial one is largely recovered as shown in (iii). This reversibility demonstrates the importance of optimized FIB lift-out to prepare lamellas for SPM characterization: the final polishing voltage is critical to manage the damage layer. Notably, lamellas can also be repolished to recover contrast and expose "fresh" surface material.

In conclusion, a FIB workflow has been demonstrated which makes it possible to examine properties of individual domain walls with a well-defined charge state in hexagonal manganites. By using *in situ* FIB lift-out, it has been possible to image the domain wall pattern on both sides before lifting out. Importantly, it has been shown that these lamellas can be prepared with sufficiently thin damage layers to resolve domains by PFM and domain wall currents by cAFM without any additional postprocessing, e.g., annealing. The effect of reducing FIB acceleration voltage (and resulting damage layer thickness) on the effective domain wall conductance has been demonstrated: it has been shown that a 5 kV polishing step drastically and reversibly improves the cAFM contrast compared to 30 kV polishing. Furthermore, by combining the possibility of estimating three-dimensional domain wall orientation from SEM with PFM and cAFM [Fig. 1(d), supplementary material Notes 1 and 2], the relation between the 3D domain wall behavior and conductivity can be investigated. These results demonstrate the general ability to work with individual improper ferroelectric domain walls and characterize their intrinsic physical properties, with the ultimate goal of developing them into atomic scale electronic components for next-generation nanotechnology.

See the supplementary material for details on determining the domain wall angle through lamellas (supplementary material Note 1), the impact of three-dimensional angles on cAFM contrast (supplementary material Note 2), and complementary cAFM data to Fig. 4 (supplementary material Fig. S3).

REFERENCES

[1]E. Salje and H. Zhang, Phase Transitions **82**, 452 (2009).

[2]G. Catalan, J. Seidel, R. Ramesh, and J. F. Scott, Rev. Mod. Phys. **84**, 119 (2012).

[3]D. Meier, J. Phys.: Condens. Matter **27**, 463003 (2015).

[4]P. S. Bednyakov, B. I. Sturman, T. Sluka, A. K. Tagantsev, and P. V. Yudin, npj Comput. Mater. **4**, 65 (2018).

[5]J. Seidel, L. W. Martin, Q. He, Q. Zhan, Y.-H. Chu, A. Rother, M. E. Hawkridge, P. Maksymovych, P. Yu, M. Gajek, N. Balke, S. V. Kalinin, S.

[6]Gemming, F. Wang, G. Catalan, J. F. Scott, N. A. Spaldin, J. Orenstein, and R. Ramesh, Nat. Mater. **8**, 229 (2009).

[6]J. Guyonnet, I. Gaponenko, S. Gariglio, and P. Paruch, Adv. Mater. **23**, 5377 (2011).

[7]M. Schröder, A. Haußmann, A. Thiessen, E. Soergel, T. Woike, and L. M. Eng, Adv. Funct. Mater. **22**, 3936 (2012).

[8]T. Sluka, A. K. Tagantsev, P. Bednyakov, and N. Setter, Nat. Commun. **4**, 1808 (2013).

[9]D. Meier, J. Seidel, A. Cano, K. Delaney, Y. Kumagai, M. Mostovoy, N. A. Spaldin, R. Ramesh, and M. Fiebig, Nat. Mater. **11**, 284 (2012).

[10]W. Wu, Y. Horibe, N. Lee, S.-W. Cheong, and J. R. Guest, Phys. Rev. Lett. **108**, 077203 (2012).

[11]R. G. P. McQuaid, M. P. Campbell, R. W. Whatmore, A. Kumar, and J. M. Gregg, Nat. Commun. **8**, 15105 (2017).

[12]Y. S. Oh, X. Luo, F.-T. Huang, Y. Wang, and S.-W. Cheong, Nat. Mater. **14**, 407 (2015).

[13]M. E. Holtz, K. Shapovalov, J. A. Mundy, C. S. Chang, Z. Yan, E. Bourret, D. A. Muller, D. Meier, and A. Cano, Nano Lett. **17**, 5883 (2017).

[14]P. Schoenherr, K. Shapovalov, J. Schaab, Z. Yan, E. D. Bourret, M. Hentschel, M. Stengel, M. Fiebig, A. Cano, and D. Meier, Nano Lett. **19**, 1659 (2019).

[15]T. Choi, Y. Horibe, H. T. Yi, Y. J. Choi, W. Wu, and S.-W. Cheong, Nat. Mater. **9**, 253 (2010).

[16]E. Ruff, S. Krohns, M. Lilienblum, D. Meier, M. Fiebig, P. Lunkenheimer, and A. Loidl, Phys. Rev. Lett. **118**, 036803 (2017).

[17]J. A. Mundy, J. Schaab, Y. Kumagai, A. Cano, M. Stengel, I. P. Krug, D. M. Gottlob, H. Doğanay, M. E. Holtz, R. Held, Z. Yan, E. Bourret, C. M. Schneider, D. G. Schlom, D. A. Muller, R. Ramesh, N. A. Spaldin, and D. Meier, Nat. Mater. **16**, 622 (2017).

[18]J. Schaab, S. H. Skjærvø, S. Krohns, X. Dai, M. E. Holtz, A. Cano, M. Lilienblum, Z. Yan, E. Bourret, D. A. Muller, M. Fiebig, S. M. Selbach, and D. Meier, Nat. Nanotechnol. **13**, 1028 (2018).

[19]T. Jungk, Á. Hoffmann, M. Fiebig, and E. Soergel, Appl. Phys. Lett. **97**, 012904 (2010).

[20]H. Pang, F. Zhang, M. Zeng, X. Gao, M. Qin, X. Lu, J. Gao, J. Dai, and Q. Li, npj Quantum Mater. **1**, 16015 (2016).

[21]L. A. Giannuzzi and F. A. Stevie, Micron **30**, 197 (1999).

[22]S. R. Burns, J. M. Gregg, and V. Nagarajan, Adv. Funct. Mater. **26**, 8367 (2016).

[23]L. W. Chang, M. McMillen, F. D. Morrison, J. F. Scott, and J. M. Gregg, Appl. Phys. Lett. **93**, 132904 (2008).

[24]A. Schilling, D. Byrne, G. Catalan, K. G. Webber, Y. A. Genenko, G. S. Wu, J. F. Scott, and J. M. Gregg, Nano Lett. **9**, 3359 (2009).

[25]R. G. P. McQuaid, L. J. McGilly, P. Sharma, A. Gruverman, and J. M. Gregg, Nat. Commun. **2**, 404 (2011).

[26]R. Ahluwalia, N. Ng, A. Schilling, R. G. P. McQuaid, D. M. Evans, J. M. Gregg, D. J. Srolovitz, and J. F. Scott, Phys. Rev. Lett. **111**, 165702 (2013).

[27]J. R. Whyte, R. G. P. McQuaid, P. Sharma, C. Canalias, J. F. Scott, A. Gruverman, and J. M. Gregg, Adv. Mater. **26**, 293 (2014).

[28]A. Schilling, T. Adams, R. M. Bowman, and J. M. Gregg, Nanotechnology **18**, 035301 (2007).

[29]S. H. Skjærvø, E. T. Wefring, S. K. Nesdal, N. H. Gaukås, G. H. Olsen, J. Glaum, T. Tybell, and S. M. Selbach, Nat. Commun. **7**, 13745 (2016).

[30]Z. Yan, D. Meier, J. Schaab, R. Ramesh, E. Samulon, and E. Bourret, J. Cryst. Growth **409**, 75 (2015).

[31]V. V. Aristov, L. S. Kokhanchik, K.-P. Meyer, and H. Blumtritt, Phys. Status Solidi A **78**, 229 (1983).

[32]R. Le Bihan, Ferroelectrics **97**, 19 (1989).

[33]A. Sogr, A. Maslovskaya, and I. Kopylova, Ferroelectrics **341**, 29 (2006).

[34]J. Li, H. X. Yang, H. F. Tian, C. Ma, S. Zhang, Y. G. Zhao, and J. Q. Li, Appl. Phys. Lett. **100**, 152903 (2012).

[35]M. Schaffer, B. Schaffer, and Q. Ramasse, Ultramicroscopy **114**, 62 (2012).

[36]C. Li, G. Habler, L. C. Baldwin, and R. Abart, Ultramicroscopy **184**, 310 (2018).

[37]N. I. Kato, J. Electron Microsc. **53**, 451 (2004).

[38]J. Huang, M. Loeffler, U. Muehle, W. Moeller, J. J. L. Mulders, L. F. T. Kwakman, W. F. Van Dorp, and E. Zschech, Ultramicroscopy **184**, 52 (2018).

[39]J. Melngailis, J. Vac. Sci. Technol., B **5**, 469 (1987).

[40]J. F. Ziegler, M. D. Ziegler, and J. P. Biersack, Nucl. Instrum. Methods Phys. Res., Sect. B **268**, 1818 (2010).